Electrochemical Immunosensors for Effective Evaluation of Amyloid-Beta Modulators on Oligomeric and Fibrillar Aggregation Processes

ARTICLE *in* ANALYTICAL CHEMISTRY · APRIL 2014

Impact Factor: 5.64 · DOI: 10.1021/ac500424t · Source: PubMed

9 AUTHORS, INCLUDING:

Ari M Chow
University of Toronto
19 PUBLICATIONS **222** CITATIONS
SEE PROFILE

Hashwin V S Ganesh
University of Toronto
8 PUBLICATIONS **30** CITATIONS
SEE PROFILE

Nan Li, Ph.D
University of Toronto
8 PUBLICATIONS **41** CITATIONS
SEE PROFILE

analytical chemistry

Article

pubs.acs.org/ac

Electrochemical Immunosensors for Effective Evaluation of Amyloid-Beta Modulators on Oligomeric and Fibrillar Aggregation Processes

Anthony J. Veloso,[†] Ari M. Chow,[‡] Hashwin V. S. Ganesh,[‡] Nan Li,[†] Devjani Dhar,[†] David C. H. Wu,[†] S. Mikhaylichenko,[†] Ian R. Brown,[‡] and Kagan Kerman*[,†,‡]

[†]Department of Physical and Environmental Sciences and

[‡]Centre for the Neurobiology of Stress, Department of Biological Sciences, University of Toronto Scarborough, 1265 Military Trail, Toronto, ON M1C 1A4, Canada

Supporting Information

ABSTRACT: A novel electrochemical immunosensor fabricated from gold compact disc electrodes was designed for rapid evaluation of aggregation processes that lead to the formation of oligomeric and fibrillar states of amyloid-beta$_{1-42}$ (Aβ_{1-42}) during Alzheimer's disease. Conformation-specific antibodies were immobilized on the surface of the gold electrode using a 3,3′-dithiobis (sulfosuccinimidyl) propionate (DTSSP) linker. Surface binding events were analyzed by electrochemical impedance spectroscopy (EIS) in which the formation of an antigen−antibody complex was quantified as a function of charge transfer resistance using a $[Fe(CN)_6]^{3-/4-}$ redox probe. The effectiveness of novel sym-triazine-derived aggregation modulators (TAE-1, TAE-2) to reduce the population of toxic oligomers was evaluated. Aβ fibril formation was validated by thioflavin T (ThT) fluorescence, whereas oligomer formation was investigated by MALDI. Antigen detection by EIS was further supported by immuno dot blot assays for oligomeric and fibrillar components. Docking simulations of the aggregation modulators TAE-1 and TAE-2 with Aβ_{1-42} fibrils performed using Autodock Vina suggest a mechanism for the improved aggregation inhibition observed for TAE-2. The results demonstrate the utility and convenience of impedance immunosensing as an analytical tool for rapid and comprehensive evaluation of effective Aβ aggregation modulating agents.

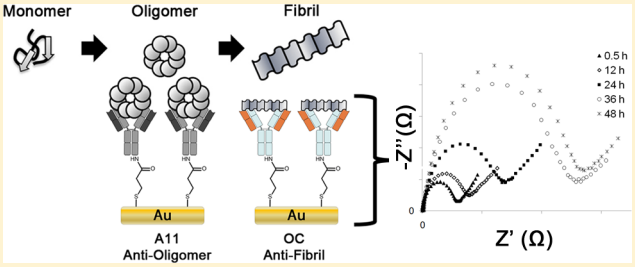

Alzheimer's disease (AD) is the most prevalent progressive dementia marked by severe impairments to memory and cognitive functions.[1,2] Current FDA-approved drug therapies for treatment of AD ameliorate the severity of dementia-related symptoms by regulating neurotransmitter dysfunctions, specifically those resulting in glutamate-induced excitotoxicity and diminishing levels of acetylcholine.[3−5] Although such strategies for therapeutic intervention have yielded moderate improvements to cognitive function, their effects are considered only temporarily beneficial as they neither prevent nor slow the rate of disease progression.[6,7] With a steady increase in the aging population, the prevalence of AD is expected to increase more than 3-fold over the next 50 years,[2] prompting urgent development of novel disease-modifying agents capable of targeting factors directly linked to neurodegeneration.

The amyloid cascade hypothesis associates the cerebral deposition of the protein amyloid beta (Aβ) with the onset and progression of AD.[8] Aβ is the prime component of neuritic plaques and occurs in two major isoforms, Aβ_{1-40} and Aβ_{1-42}, which exhibit differential rates of spontaneous self-association into supramolecular assemblies forming fibrils and later plaques.[9,10] Although Aβ_{1-40} is natively present in higher quantities, Aβ_{1-42} exhibits faster rates of aggregation, generates more free radical damage, and is considered the more neurotoxic of the two species. Higher order Aβ aggregates induce an immunological response in the brain, recruiting microglia that release pro-inflammatory cytokines, including tumor necrosis factor-α, interlukin-6, and interlukin-1β. Despite being initially beneficial, deleterious effects ultimately occur as a result of their chronic activation.[11−13] Smaller soluble oligomers have been identified as the primary conformation of neurotoxic Aβ, whose formation correlates more closely to the severity of dementia than fibril or plaque load.[14−16] One mechanism for oligomer-induced toxicity is their incorporation into the lipid bilayer of neuronal cells, which results in disruption of membrane homeostasis by unregulated influx of Ca^{2+} ions and excessive membrane depolarization.[17−20] The increase of intracellular Ca^{2+} enhances the formation of reactive oxygen species (ROS), facilitates neurotransmitter excitotoxicity, and cumulatively accelerates neuronal death.[21] A reduction of amyloid burden by inhibition of Aβ production, modulation of toxic oligomers formation, or enhancement of toxic oligomer clearance could result in disease-modifying effects.[22]

The effectiveness of Aβ aggregation modulators is commonly measured by their capacity to dissociate or inhibit fibril assembly.[23−28] However, modulated growth of Aβ fibrils would

Received: January 15, 2014
Accepted: April 6, 2014
Published: April 6, 2014

   dx.doi.org/10.1021/ac500424t | *Anal. Chem.* 2014, 86, 4901−4909

result in a shift in aggregate equilibrium that may facilitate further formation of toxic oligomeric species.[29] Thus, a more accurate evaluation of aggregation modulators requires careful analysis of their effects on the formation of both oligomeric and fibrillar aggregates. We synthesized a small library of sym-triazine derivatives capable of multitarget modulation of Aβ fibrils and acetylcholinesterase activity.[30] Significantly, compounds TAE-1 and TAE-2 (Figure S1) exhibited additional beneficial effects on cultured human neurons, promoting differentiation and the extension of neurite processes that could potentially counteract AD-mediated neurodegenerative effects and promote neuronal survival.[31] Analysis of fibril formation by transmission electron microscopy indicates that TAE-1 and TAE-2 redirect Aβ by the formation of off-pathway aggregates, the nature of which are explored within this study.[30]

A11 is a conformation-specific Aβ antibody that selectively binds to neurotoxic oligomeric intermediates of Aβ.[32−34] Oligomers that are structurally remodeled in the presence of aggregation disrupting agents have exhibited reduced quantities of the A11 reactive epitopes and correspondingly lower toxicities.[35,36] In this report, A11 interactions with neurotoxic oligomers are compared with the fibril-specific antibody, OC, to assess the capacity of sym-triazine derivatives to reduce the toxicity of Aβ aggregates.[33] Time-dependent analysis of aggregate formation was evaluated by electrochemical impedance spectroscopy (EIS) on gold CD electrodes. EIS is a sensitive technique for label-free transduction of binding events at an electrode surface.[37−39] Oligomeric or fibrillar aggregates of Aβ were captured via immunological interactions with their corresponding antibodies (A11 or OC) immobilized on the electrode surface. The degree of surface binding was subsequently determined by measuring the charge-transfer resistance of a ferri-ferrocyanide ($[Fe(CN)_6]^{3-/4-}$) redox probe. Herein, we apply EIS using conformation specific antibodies to evaluate the effects of our novel sym-triazines modulators, TAE-1 and TAE-2, on the distribution of fibrillar and toxic oligomeric species of $A\beta_{1-42}$.

EXPERIMENTAL SECTION

Electrochemical Immunosensor Construction. The construction of the individual layers of the immunosensor is represented in Figure S2. The Kodak gold preservation archival grade CDs used in the preparation of the working electrode consisted of a gold film (50−100 nm thickness) deposited onto a photosensitive layer above a hard shell polycarbonate disc.[40,41] The gold surface was further coated in a protective polymer that was removed using concentrated nitric acid (5 mL), which was applied to the CD surface for 10 min followed by rinsing with 18.2 MΩ water.[42] A rectangular section (approximately 1 cm × 4 cm) of the CD was cut out. A hole puncher with an area of 2 mm^2 was used to create a hole in a strip of adhesive insulating tape. The tape was then applied to the bare gold surface to isolate the working area of the electrode. During long periods of storage, oxides are known to accumulate over the exposed gold surface.[40] To prevent this, CD electrodes were prepared as needed.

Prior to electrode modification, surface impurities of the CD electrodes were removed by performing cyclic voltammetry (CV) between 0.0 and 1.5 V (vs Ag/AgCl) at a scan rate of 100 mV s^{-1} in sulfuric acid (0.5 M), followed by rinsing with 18.2 MΩ water.[41] Immobilization of conformation-specific antibodies onto the gold CDs was achieved using the homobifunctional linker, 3,3′-dithiobis (sulfosuccinimidyl) propionate (DTSSP), which contains both a gold-reactive thiol unit as well as an amine-reactive *n*-hydroxy sulfosuccinimide group for covalent antibody attachment.[43] Formation of the DTSSP film was achieved by depositing a 20 μL aliquot of 2 mM DTSSP (prepared in 100 mM Na_2CO_3, pH 8.5) onto the surface of the gold working electrode overnight at 4 °C.[43,44] Excess DTSSP was removed by rinsing with Na_2CO_3 followed by the addition of 20 μL of the A11 (5 in 1500) or OC (1 in 1500) OC antibodies for 1 h at room temperature 24 ± 1 °C. Unreacted *N*-hydroxy(sulfo) succinimide active esters were blocked using 0.1 M ethanolamine for 1 h at room temperature followed by rinsing in 50 mM phosphate-buffered saline (PBS) pH 7.4 100 mM NaCl.

Electrochemical Analysis. Electrochemical measurements were performed using a μAutolab-III potentiostat (Metrohm, The Netherlands) in a three-electrode configuration composed of a gold CD working electrode, platinum counter electrode, and Ag/AgCl reference electrode (in 3 M KCl). CV measurements were controlled using the General Purpose Electrochemical System (GPES) software and the Frequency Response Analysis (FRA) system software, respectively. For characterization of stepwise layer formation on the gold electrode surface, CVs were carried out from −0.25 to 0.6 V (vs Ag/AgCl) in $[Fe(CN_6)]^{3-/4-}$ (5 mM in 10 mM KCl) at a scan rate of 100 mVs^{-1}.[43] EIS was performed over a frequency range of 0.1 to 100 000 Hz with 0.005 V amplitude (rms). Impedance data was fit to a Randles Equivalent Circuit model using FRA to determine changes in charge transfer resistance (R_{CT}) resulting from modifications to the electrode surface. For the detection of Aβ fibrils and oligomers, binding was reported as ΔR_{CT}, in which the R_{CT} of the ethanolamine blocked surface was subtracted from the R_{CT} measured for Aβ samples.[45]

RESULTS AND DISCUSSION

Step-Wise Electrochemical Characterization of Immunosensor Layers. In recent years, electrochemistry has been applied as a promising method to study the aggregation of neurodegenerative proteins including Aβ[46] and α-synuclein[47,48] related to Alzheimer's disease (AD) and Parkinson's disease, respectively. In this study, electrochemical impedance spectroscopy (EIS) of amyloid beta (Aβ) was conducted on gold compact disk (CD) electrodes. Technologies for "bioCDs" have recently been developed primarily as low cost optical microarray chips.[49−52] Thin gold films can be reproducibly generated during CD fabrication and are thus attractive as they circumvent the need to purchase costly metallic sputtering equipment, do not require further postprocessing and polishing, and multiple electrode units can be derived from a single CD.[41]

Cyclic voltammetry (CV) and EIS were used to study successive layer formation of the immunosensor. CVs shown in Figure 1a denote the kinetics of electron transfer marked by discrete changes in peak current and the separation of peak potentials. Comparatively, EIS spectra (Figure 1b) were used to determine the charge transfer resistance (R_{CT}) at the electrode surface, extrapolated from the diameter of a semicircle generated by the Nyquist plot. The bare unmodified electrode, Figure 1, curve i, was characterized by fast electron transfer kinetics, limited primarily by $[Fe(CN_6)]^{3-/4-}$ diffusion to the surface. Accordingly, CVs showed small separation between anodic and cathodic peak potentials, corresponding to the high reversibility of the redox process, whereas the EIS spectrum was showed only small R_{CT} and long tail denoting diffusion of the

dx.doi.org/10.1021/ac500424t | Anal. Chem. 2014, 86, 4901−4909

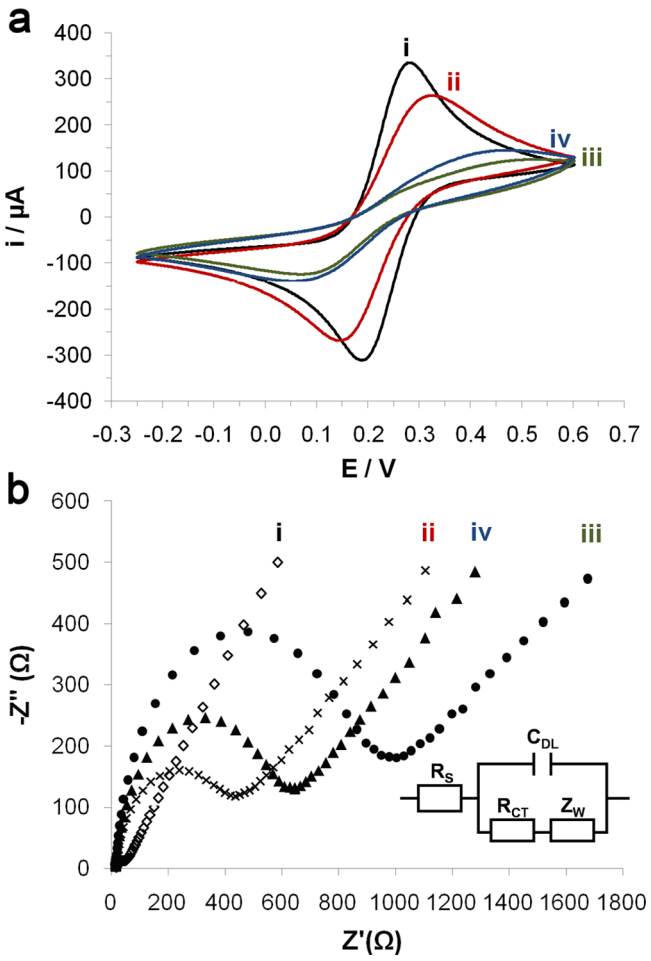

Figure 1. Cyclic voltammograms (a) and Nyquist plots (b) showing the step-wise modification of a gold CD working electrode surface obtained for bare gold CD (curve i), DTSSP-gold CD (curve ii), antioligomer A11-DTSSP-gold CD (curve iii), and ethanolamine-blocked-A11-DTSSP-gold CD (curve iv). Electrochemical measurements were performed in 10 mM $[Fe(CN)_6]^{3-/4-}$ prepared in 0.1 M KCl. EIS was analyzed over a frequency range of 0.1 Hz−10 kHz, and R_{CT} values were interpreted by Randles equivalent circuit model (inset). Cyclic voltammograms were measured at a scan rate of 100 mV s^{-1}.

redox probe. Formation of the DTSSP film (Figure 1 curve (ii)) leads to an increase in both peak separation and charge transfer resistance, which were further increased upon addition of both the A11 antibody (Figure 1, curve iii, and OC antibody Figure S3, curve i). Interestingly, blocking of unreacted succinimide units by ethanolamine (Figure 1, curve iv, and Figure S3, curve ii) resulted in an opposing decrease in R_{CT} as well as peak. It has been suggested that this phenomenon may be due to the displacement of noncovalently immobilized antibodies by the blocking groups, effectively causing their replacement by smaller ethanolamine groups.[43]

Detection of Fibrils and Toxic Aβ Oligomers by EIS and Immuno Dot Blot. Modulated aggregation of $A\beta_{1-42}$ by TAE-1 and TAE-2 was studied by time-dependent EIS analysis measured at 12 h intervals over 48 h. Aβ aggregation was stimulated by incubation at 37 °C in 50 mM PBS pH 7.4. At each measurement time point, EIS was performed using the two conformation specific antibodies to measure fibril and toxic oligomer distribution changes over time (Scheme 1). The A11 antibody specifically recognizes the toxic epitopes of oligomers

Scheme 1. Detection Principle for Monitoring $A\beta_{1-42}$ Fibrils and Toxic Oligomers Using Conformation Specific Antibodies in Conjunction with EIS[a]

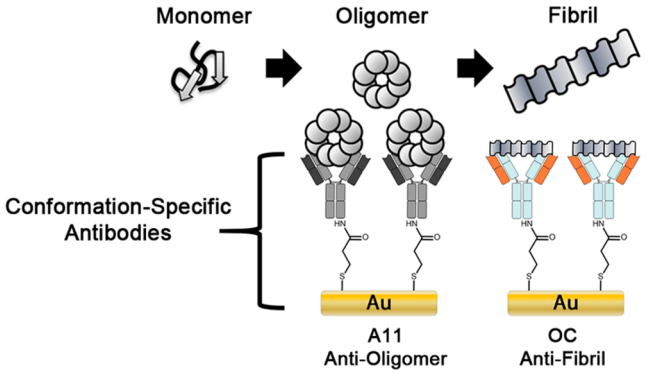

[a]Anti-fibril (OC) and anti-oligomer (A11) antibodies are covalently immobilized onto separate gold CD electrodes. $A\beta_{1-42}$ aggregation was stimulated by incubation at physiological conditions and at various time points; an aliquot of the incubating solution is analyzed by both the A11 and OC immunosensors to determine the distribution of oligomers and fibrils over time.

of amyloidogenic proteins, including Aβ, insulin, and prion proteins, but it does not bind to fibrillar or low molecular weight species.[32] Consequently, reduced binding of A11 antibodies has been linked to lowered oligomer toxicity within modulated aggregates of Aβ.[35,36] Similarly, OC antibody reacts with the fibrils of various amyloid-type proteins but not with prefibrillar oligomers or native monomeric conformations.[33] Thus, combination analysis with both antibodies by electrochemical immunosensing provides a rapid, comprehensive means to evaluate agents capable of impeding toxic pathways of Aβ assembly.

Time-dependent Nyquist plots of $A\beta_{1-42}$ measured using the fibril-specific OC and oligomer-specific A11 antibodies are shown in Figure 2a,b, respectively. Similarly, the Nyquist plots for TAE-1- and TAE-2-treated samples are shown in Figure S4. Each Nyquist plot is characterized by a semicircular arc, the diameter of which corresponds to charge-transfer resistance (R_{CT}) at the electrode surface. An increase in R_{CT} was associated with an increased binding of the appropriate antigen (fibril or oligomer) to its respective antibody on the immunosensor surface. A strict comparison of R_{CT} values extrapolated from the Nyquist plots OC and A11 immunosensors (Figure 2 and Figure S4) may be better represented as bar graphs in Figure 3a,b, respectively. ΔR_{CT} is the difference in R_{CT} between the antigen-bound layer and the base antibody layer. Figure 3a shows the distribution of fibrils for $A\beta_{1-42}$ as well as in the presence TAE-1 and TAE-2 at equimolar concentration. For $A\beta_{1-42}$ using the OC immunosensor, a gradual increase in R_{CT} was observed corresponding to the increase in fibril formation with the highest R_{CT} measured at 48 h, after which saturation occurs. The observed trend in aggregation corresponded well with the predicted nucleation-dependent model for Aβ fibril formation processes. Conversely, TAE-treated conditions showed both a longer lag phase as well as decreased fibril binding to the OC immunosensor surface, resulting in a lower R_{CT} relative to the control after 48 h. Whereas fibril formation appeared to increase continuously up to 48 h for TAE-1, TAE-2 showed a drop in fibrillar content between 36 and 48 h, indicating modulation of fibrils post formation. This is in agreement with previous reports of the

dx.doi.org/10.1021/ac500424t | Anal. Chem. 2014, 86, 4901−4909

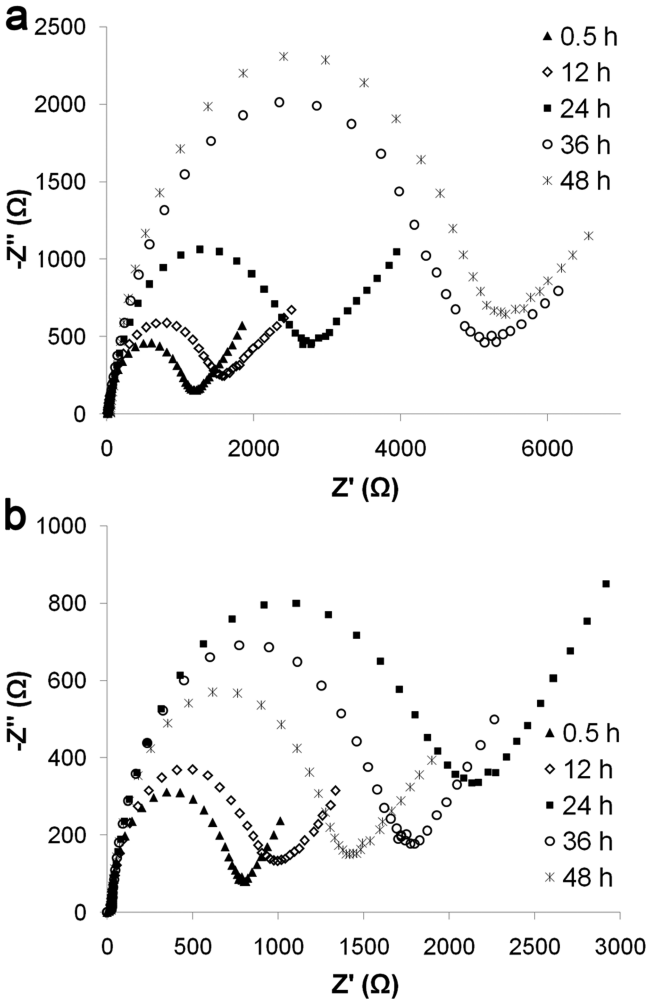

Figure 2. EIS analysis of Aβ_{1-42} aggregation by (a) fibril-specific OC and (b) oligomer-specific A11 antibody-modified gold CD electrodes shown as Nyquist plots. Hexafluoro-2-propanol (HFIP)-monomerized Aβ_{1-42} (5 μM) was incubated at 37 °C over 48 h in 50 mM PBS, 100 mM NaCl, pH 7.4. EIS measurements were performed at 0.5, 12, 24, 36, and 48 h time periods using two separate conformation-specific immunosensor configurations. Corresponding R_{CT} values were determined by fitting with Randles equivalent circuit and plotted in plot b (antifibril, OC) and plot b (antioligomer, A11), respectively.

improved capacity of TAE-2 to dissociate fibrils.[30,31] For the A11 immunosensor, R_{CT} appeared to peak at approximately 24 h, corresponding to substantial oligomer formation, and then dropped at the 36 and 48 h time points, when fibril formation was expected to dominate. Notably, both TAE-1 and TAE-2 appeared to induce comparable levels of oligomer suppression, as indicated by both the low and relatively constant ΔR_{CT} values.

To further support the EIS data, immuno dot blot assays were performed using the OC antibody (Figure 4a). In general, the overall trend in fibril inhibition measured using the OC antibody is consistent between the EIS and immuno dot blot assay. Specifically, the Aβ_{1-42} control showed the highest fibril signal starting at 24 h that increased gradually over time, whereas TAE-treated samples appeared to reduce the fibrillar content at all time points. This was evident by the decrease in immunoblot intensity, which signifies less antibody binding to the fibrillar antigen. Specifically, in the TAE-1 treatment, fibril binding was detectable beginning at 48 h, whereas TAE-2 showed significant modulation of fibrils even up to 48 h. Particularly, in EIS plots at the saturation phase (48 h), the fibril binding detected for the TAE-2 condition appeared to be significantly lower than TAE-1, suggesting a larger degree of fibril modulation consistent with previous data.[31] Interestingly, in some cases, particularly at earlier time points, the binding of fibrils to the immunosensor surface detected by EIS preceded the observable fibril binding on the dot blot. Specifically, binding of antigens detected below a threshold of approximately 1 kΩ ΔR_{CT} using EIS was not observed in the immuno dot blot staining. Thus, the immuno dot blot allows for detection of a fibril signal equivalent or above an approximate threshold of 1500 Ω, as measured by the EIS immunosensor. This suggests lower sensitivity in the dot blot assay requiring an increased amount of loaded materials for detection. This property is readily apparent in TAE-treated conditions, in which the content of fibrils is significantly decreased (Figure 4a). However, in view of Figure 3a, we observe that the overall trend of fibril formation and inhibition by TAE-1 and TAE-2, as detected by dot blot, matches the pattern observed by the EIS immunosensor. This demonstrated reliability of the immunosensor system in detecting the kinetics of oligomer and fibril formation.

Conversely, analysis of oligomeric species using A11 immuno dot blot assays (Figure 4a) showed no significant band pattern at a loading volume of 50 μL. However, EIS showed a distinct increase in R_{CT} at 24 h in the Aβ_{1-42} control, which was associated with the phase at which point oligomer species were most prominent. Significantly, TAE-1 and TAE-2 conditions were found to suppress the formation of this peak at 24 h with no significant oligomer binding detected for either condition from EIS analysis. As described for the OC antibody studies, this lack of oligomer detection was attributed to the differential sensitivity of dot blot versus the immunosensor system. To confirm this hypothesis, oligomer samples measured at 24 h were analyzed by dot blot using increasing loading volumes (50, 200, and 400 μL). The increased amount of total protein was monitored using Ponceau S and Amido Black staining methods (Figure 4b). Interestingly, immuno dot blot assay only allowed detection of oligomer species at sample volumes of 200 μL, suggesting that Aβ_{1-42} oligomer kinetics can be studied at concentration that are at least 4-fold lower than currently techniques using the EIS-based immunosensor. The larger dynamic range of the EIS-based immunosensors allows for parallel detection of fibrils and oligomers at the same volume of 50 μL, whereas the dot blot requires larger volumes for oligomer detection that would overload and exceed the reliable detection threshold for fibrils. The faster detection times achieved using EIS immunosensors provides a significant advantage over the traditional dot blot approach, as employed by previous studies measuring toxic aggregate modulation.[53,54]

Comparative Analysis of Aβ Aggregation by ThT Fluorescence and MALDI. The effective modulation of fibrillar Aβ_{1-42} aggregates observed by EIS and dot blot immunoassays was validated by simultaneous analysis with thioflavin T (ThT) fluorescence and matrix-assisted time-of-flight (MALDI-TOF) mass spectrometry (MS). ThT is a fluorescent, β-sheet binding benzothiazole dye, and emission at 485 nm corresponds to fibril formation within amyloid proteins. The spontaneous self-association of Aβ is commonly described by a nucleation-dependent polymerization model,[11] in which the appearance of a stable nuclei serves as a template for the successive addition of Aβ monomers that contribute to

dx.doi.org/10.1021/ac500424t | Anal. Chem. 2014, 86, 4901−4909

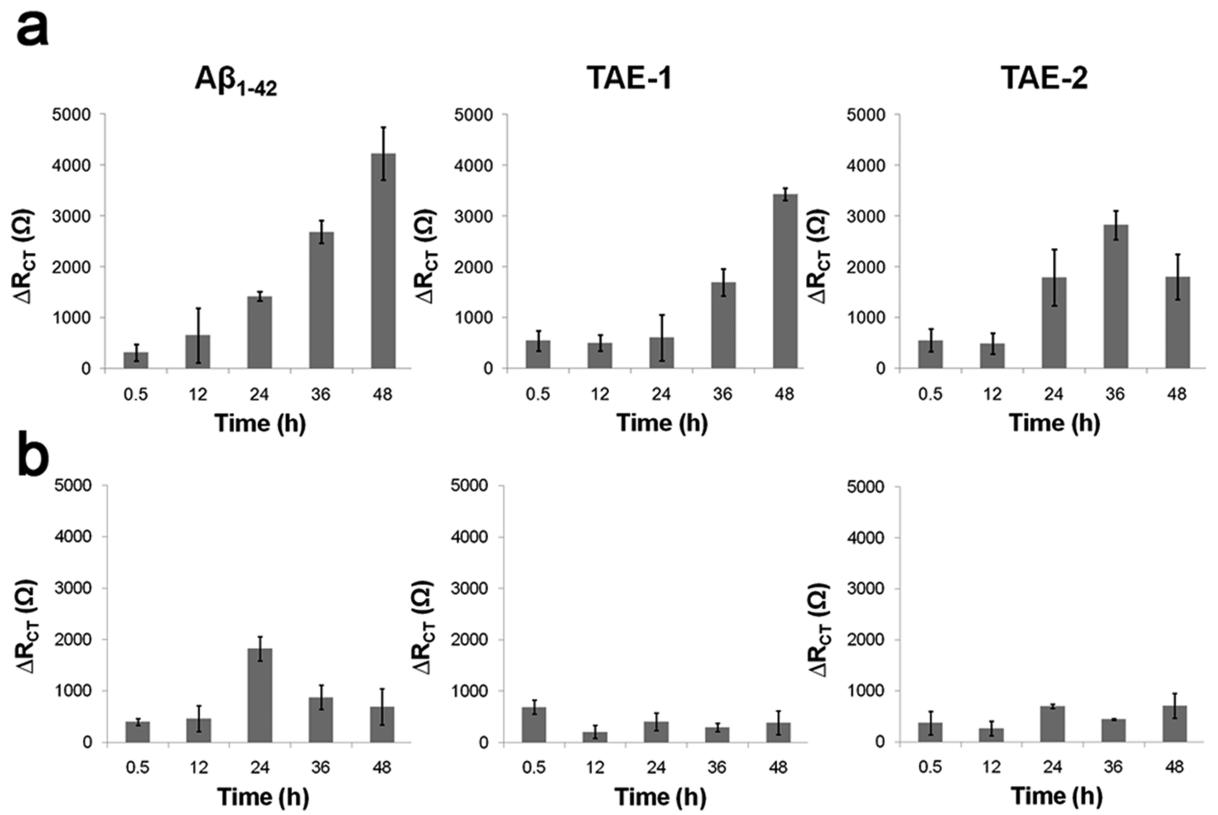

Figure 3. Kinetic analysis of Aβ_{1-42} aggregation in the presence of the sym-triazine modulators TAE-1 and TAE-2 by EIS using conformation-specific (a) antifibril "OC" and (b) antioligomer "A11" antibodies. Aβ_{1-42} (5 μM) was incubated at 37 °C alone and with equimolar concentration of TAE-1 and TAE-2 in 50 mM PBS, 100 mM NaCl, pH 7.4. ΔR_{CT} values were obtained for 0.5, 12, 24, 36, and 48 h. Error bars for EIS denote the standard deviation obtained for $n \geq 3$ measurements performed on independent gold CD electrodes.

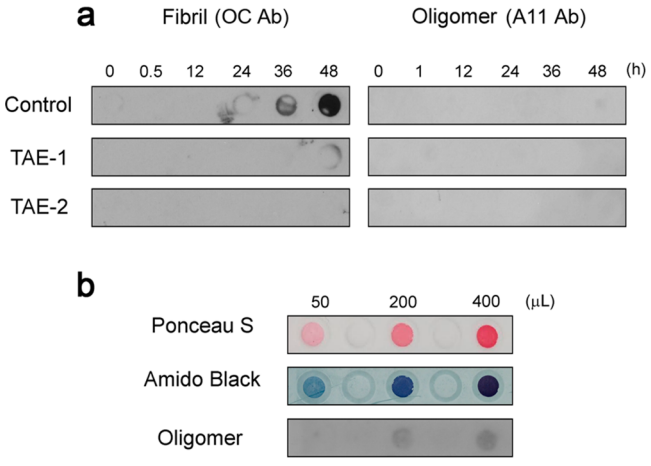

Figure 4. (a) Kinetic analysis of Aβ_{1-42} aggregation in the presence of sym-triazine modulators TAE-1 and TAE-2 by immuno dot blot assays using conformation-specific antibodies for fibril (OC) and oligomer (A11) components. Aβ_{1-42} (5 μM) was incubated at 37 °C alone and with equimolar concentration of TAE-1 and TAE-2 in 50 mM PBS, 100 mM NaCl, pH 7.4. At the indicated time points, aliquots of the incubating stock was removed and analyzed by dot blot assay. (b) Ponceau S and Amido Black staining show increasing protein content as a function of loading volume for 50, 200, and 400 μL. EIS-detectable oligomers formed at 24 h were observed only in loading volumes above 200 μL using a higher intensity ECL substrate.

fibril elongation until depletion of the monomer reservoir. This predicted model of fibril formation is consistent with the sigmoidal growth pattern observed by ThT for Aβ_{1-42} controls (Figure S5). Following addition of the sym-triazine modulators, TAE-1 and TAE-2, at equimolar concentration to Aβ_{1-42}, we observed an extension of the lag phase as well as a significant drop in fluorescence intensity relative to the uninhibited control for each measured time point, indicative of a disruption to the native fibril assembly kinetics. Notably, fluorescence, EIS and immuno dot blot confirmed that TAE-2-treated samples were found to enter the growth phase prior to those treated by TAE-1. However, Aβ_{1-42} fibrils formed in these TAE-2-treated condition subsequently underwent a disassembly at approximately 36 h resulting in a lower fluorescence signal compared to TAE-1 at the saturation phase. Specifically, fibril inhibition values of 22.9% and 48.0% were measured after 48 h incubation with TAE-1 and TAE-2, respectively, comparable with previously reported values.[30,31] We note that ThT fluorescence data may be subjected to false positives, as the presence of modulating compounds could potentially compete for dye binding sites, resulting in an apparent decrease in fluorescence intensity that is not caused by fibril inhibition.[55] Accordingly, EIS and immuno dot blot assays were designed to circumvent these issues by directly capturing Aβ_{1-42} fibrils via conformation-specific OC antibodies. Comparative analysis showed that the kinetic curves measured by ThT fluorescence matched closely with both EIS and dot blot data at numerous time points, supporting the validity of the ThT assay for monitoring TAE-mediated fibril inhibition.

In addition to the inhibitive effects of TAE-1 and TAE-2 on classic Aβ fibril assembly, we have previously demonstrated that both sym-triazines remodel Aβ to form amorphous aggregate structures that lack conventional fibrillar architecture.[30] To

dx.doi.org/10.1021/ac500424t | Anal. Chem. 2014, 86, 4901−4909

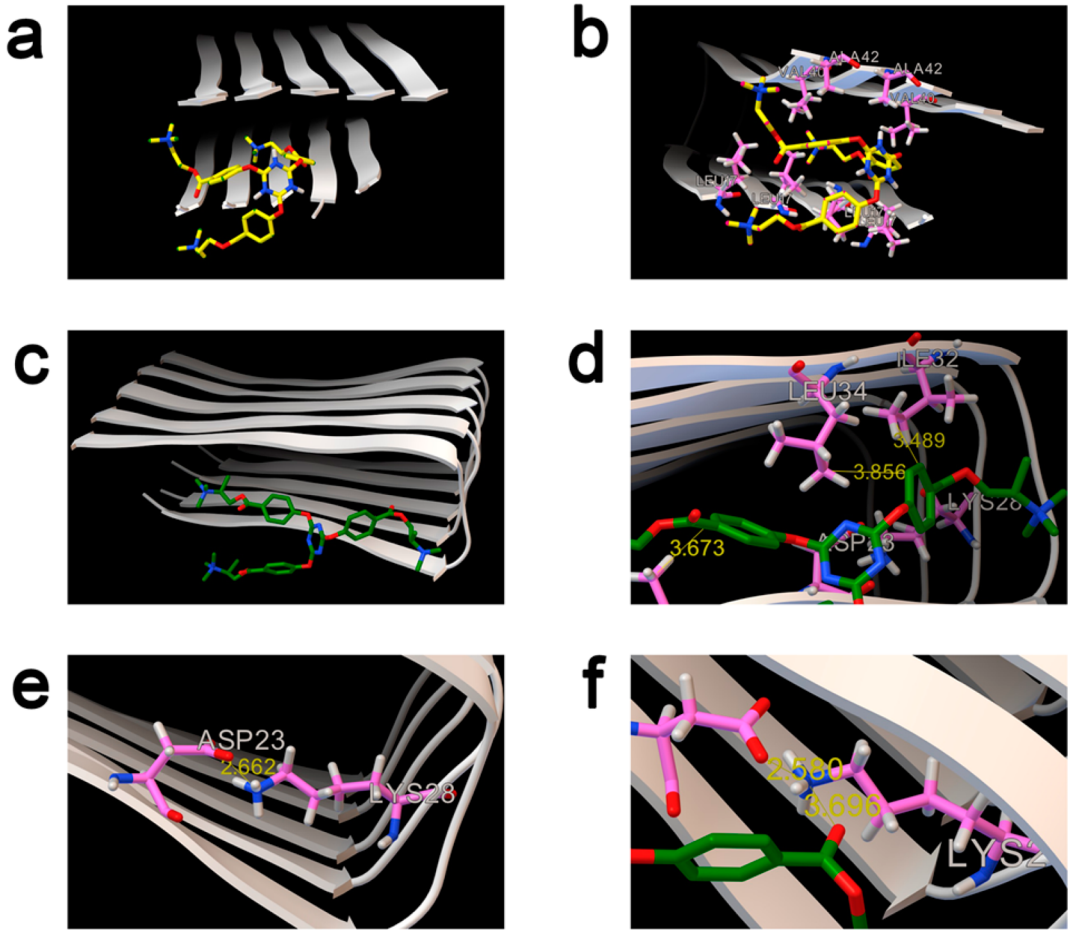

Figure 5. Molecular modeling simulations to determine the binding affinities of TAE-1 (a, b) and TAE-2 (c, d) to Aβ_{1-42} fibrils (2BEG)[57] using Autodock Vina run at an exhaustiveness of 400. The models depicted here for TAE-1 and TAE-2 represent the conformations of highest binding affinity, evaluated by binding energy (ΔG_b, kcal/mol). TAE-1 (−6.2 kcal/mol) associated with the terminal hydrophobic residues of the Aβ_{1-42}, whereas TAE-2 (−6.7 kcal/mol) demonstrated a stronger binding affinity and interacted more closely with the central hydrophobic residues. (a, c) Show the Autodock-predicted binding modes for TAE-1 and TAE-2, respectively, with (b, d) depicting the closely interacting hydrophobic residues. (e) Highlights the location of the Asp23−Lys28 salt bridge, integral to the formation of the β-sheet turn. (f) Shows potential disruption of the last bridge by the binding of TAE-2.

further evaluate the presence of these amorphous assemblies, we performed simultaneous analysis of Aβ_{1-42} interactions with TAE-1 and TAE-2 by MALDI-TOF MS (Figure S6). Using a method adapted from Zovo and co-workers,[55] the formation of large supramolecular assemblies of Aβ, such as fibrils, could be determined by monitoring the rate of decrease of the Aβ_{1-42} monomer peak. As previously mentioned, during the exponential growth phase, the monomer reservoir becomes depleted as they associate with the terminal branches rapidly elongating fibrils. Interestingly, in the presence of certain fibril-inhibiting agents, disruption of this assembly process causes the monomer peak to be maintained.[55] We have applied this approach to characterize the effects of TAE-1 and TAE-2 on the formation of Aβ_{1-42} assemblies.

For each time point measurement, an aliquot of Aβ_{1-42} was removed from the incubation and mixed with a CHCA MALDI matrix at a 1:2 ratio, spotted onto a stainless steel plate then dried by nitrogen gas. MALDI measurements were averaged from random 5 points within the spotted region and the monomer peak was observed at 4515.26 m/z. Over increasingly longer incubation periods, the formation of larger aggregates resulted in a gradual decrease in the monomer peak of Aβ_{1-42}. Complete disappearance of the Aβ_{1-42} monomer peak was found to occur after 24 h corresponding to the onset of the elongation phase (Figure S6a), as determined by ThT fluorescence.[55] We hypothesize on the basis of previous studies[30] that the more rapid disappearance of the monomer peak in TAE-1 and TAE-2 treated samples occurred due to the formation of off-pathway aggregates that are capable of accumulating monomers at a faster rate compared to Aβ alone. The toxicity of these off-pathway aggregates are currently being studied by our group (Figure S6b,c).

However, the complete disappearance of the monomer peak in TAE-treated samples also preceded observable fibril formation, as measured by ThT, EIS, and immuno dot blot. Furthermore, MALDI MS analysis was performed over a mass range of 1500 to 40 000 Da for both TAE conditions. Analysis conducted over 24 h showed no observable low molecular weight multimeric structures (e.g., dimers, trimers) with Aβ. We suggest that the rapid drop in the monomer peak intensity of the Aβ_{1-42} may have resulted from TAE-mediated incorporation into larger (>40 kDa), nonfibrillar assemblies. This hypothesis supports our previous report that TAE-1 and TAE-2 interact with Aβ to form large amorphous aggregates.[30] In order to gain insights into the interactions of TAE-1, TAE-2

dx.doi.org/10.1021/ac500424t | Anal. Chem. 2014, 86, 4901−4909

with $A\beta_{1-42}$, binding affinity studies were performed using in silico molecular docking simulations.

Molecular Docking Simulations of TAE-1 and TAE-2 with $A\beta_{1-42}$ Fibrils. Although TAE-1 and TAE-2 possess comparable structures composed of a sym-triazine core with benzene-containing quaternary amine substitutions, notable differences in their capacity for fibril inhibition have been observed by transmission electron microscopy, ThT fluorescence spectroscopy[30,31] and, in the present report, by EIS. It has previously been suggested that the additional methyl substituents of TAE-2 improved intercalation into the hydrophobic residues of $A\beta$ thereby increasing fibril inhibition by disrupting native assembly self-assembly mechanisms.[30,56] In order to provide better understanding of these mechanisms, molecular docking simulations (Figure 5) were performed for TAE-1 and TAE-2 individually with $A\beta_{1-42}$ fibril models obtained from Luhrs et al.[57] Autodock Vina is a virtual screening tool used to predict the binding affinity of small ligands to receptors of defined three-dimensional structure.[58,59] The output is a series of lowest energy docking conformations represented as three-dimensional models with their corresponding binding energies (ΔG_b) given in kcal/mol. Generally, a lower binding energy corresponds to higher binding affinity, because the lower energy denotes a stability resulting from the interaction.[59] However, sites that demonstrate a greater population of potential binding conformations have been shown to be better predictors of natively observed states.[58]

Figure 5a,c depict the binding location of TAE-1 and TAE-2, respectively, on a fibril model of $A\beta_{1-42}$. TAE-2 demonstrated higher affinity for $A\beta_{1-42}$ with a binding energy of −6.7 kcal/mol. TAE-1 was found to have a slightly weaker binding energy of −6.2 kcal/mol. Despite comparable Autodock scores, the preferred docking sites of both inhibitors differed significantly. This has been attributed to the fact that TAE-1 interacted more closely with terminal hydrophobic residues of the $A\beta_{1-42}$ fibril (Val30, Val40, Ile41, and Ala42) (Figure 5b). Conversely, the preferred docking site of TAE-2 was close to the central hydrophobic residues (Val24, Ile32, Leu34, and Val36) (Figure 5d). The hydrophobic residues of both central and terminal regions of the $A\beta$ fibril have been identified as integral components for intramolecular stabilization of the β-sheet.[60] Accordingly, destabilization of either site by TAE-1 or TAE-2 is a likely mechanism through which fibril inhibition may occur. Additionally, the greater number of residues contributing to the central hydrophobic region (Val18, Phe20, Ile31, Ile32, Gly33, Leu34, Met35, Val36) is expected to have a greater stabilizing effect, and preferred targeting of this region by TAE-2 would account for the improved inhibitory effects. Furthermore, Figure 5e shows an Asp23−Lys28 salt bridge that plays an integral role in the formation of the β-sheet turn. Potential disruption of this interaction by TAE-2 (Figure 5f) may serve as an additional contributor to the improved activity of this compound. The binding energies and primary interactions of TAE-1 and TAE-2 with $A\beta_{1-42}$ fibrils are summarized in Table S1. Although the accuracy of binding affinity predictions determined using Autodock Vina have improved substantially over previous Autodock iterations, errors of up to ±2 kcal/mol remain possible. Autodock Vina therefore should not be employed as the only criterion for ligand selection and evaluation.[59] Nevertheless, the predicted conformations reported here strongly support previously reported data describing the differential inhibitory effects of TAE-1 and TAE-2.[32,33]

CONCLUSIONS

In summary, we report a novel impedance approach that uses conformation-specific antibodies (OC and A11) to monitor the change in distribution of fibrillar and oligomeric $A\beta$ during stimulated aggregation. Results indicate that in the presence of sym-triazines, TAE-1 and TAE-2, the native fibril formation kinetics of $A\beta_{1-42}$ were disrupted, resulting in a decrease in total fibril content. Additionally, both TAE-1 and TAE-2 were found to significantly reduce the presence of the A11-reactive oligomer epitopes, suggesting a potential reduction of $A\beta$ toxicity. EIS results were supported by ThT fluorescence, MALDI TOF MS, and immuno dot blot assays. The differential activity between TAE-1 and TAE-2 was further explored via molecular docking simulations. TAE-1 was found to bind closely to the terminal hydrophobic residues of the $A\beta_{1-42}$ fibril (−6.2 kcal/mol), whereas TAE-2 bound more strongly to the central hydrophobic region (−6.7 kcal/mol). In addition, TAE-2 exhibited the potential to disrupt the Asp23−Lys28 salt bridge, which is integral to the assembly of the β-sheet turn, thereby contributing to its improved inhibition activity. The use of EIS in combination with conformation-specific antibodies provides a comprehensive method to evaluate the effectiveness of aggregation modulators by monitoring the formation of toxic $A\beta$ assemblies. This promising technology should enhance the screening of viable $A\beta$-targeted drug therapies for Alzheimer's disease.

ASSOCIATED CONTENT

Supporting Information

Chemical reagents and detailed experimental procedures for immuno dot blot assay, molecular docking simulations, ThT fluorescence, and MALDI-TOF MS. This material is available free of charge via the Internet at http://pubs.acs.org.

AUTHOR INFORMATION

Corresponding Author

*E-mail: kagan.kerman@utoronto.ca. Fax: +1 416 287 7279. Tel.: +1 416 287 7249.

Author Contributions

A.J.V., A.M.C., I.R.B., and K.K. wrote the manuscript. D.D. and S.M. synthesized the aggregation modulators. A.M.C. and H.V.S.G. performed immunodetection of $A\beta$ by dot blot. A.J.V., N.L., and D.C.H.W. constructed CD sensors and performed immunodetection of $A\beta$ by electrochemical impedance spectroscopy. A.J.V. and D.C.H.W. performed MALDI, ThT fluorescence, and molecular modeling analysis.

Notes

The authors declare no competing financial interest.

ACKNOWLEDGMENTS

This work was conducted with the support of NSERC Discovery Grants to K.K. and I.R.B., a Canada Research Chair (Tier I) in Neuroscience to I.R.B., as well as a Biomedical Young Investigator Award from the Alzheimer Society of Canada to K.K. We thank Tony Adamo of the Teaching and Research in Analytical Chemical and Environmental Science (TRACES) Centre at the University of Toronto Scarborough for expertise and assistance in performing MALDI analysis of $A\beta$.

REFERENCES

(1) Sperling, R. A.; Aisen, P. S.; Beckett, L. A.; Bennett, D. A.; Craft, S.; Fagan, A. M.; Iwatsubo, T.; Jack, C. R.; Kaye, J.; Montine, T. J.; Park, D. C.; Reiman, E. M.; Rowe, C. C.; Siemers, E.; Stern, Y.; Yaffe, K.; Carrillo, M. C.; Thies, B.; Morrison-Bogorad, M.; Wagster, M. V.; Phelps, C. H. *Alzheimer's Dementia* **2011**, *7*, 280−292.

(2) Alzheimers Disease International. World Alzheimer's Report 2012: Overcoming the Stigma of Dementia, Alzheimer's Disease International. http://www.alz.co.uk/ (accessed March 14, 2014).

(3) Dong, X. X.; Wang, Y.; Qin, Z. H. *Acta Pharm. Sinica* **2009**, *30*, 379−387.

(4) Tayeb, H. O.; Yang, H. D.; Price, B. H.; Tarazi, F. I. *Pharmacol. Ther.* **2012**, *134*, 8−25.

(5) Mohapel, P.; Leanza, G.; Kokaia, M.; Lindvall, O. *Neurobiol. Aging* **2005**, *26*, 939−946.

(6) Raschetti, R.; Maggini, M.; Sorrentino, G. C.; Martini, N.; Caffari, B.; Vanacore, N. *Eur. J. Clin. Pharmacol.* **2005**, *61*, 361−368.

(7) Raina, P.; Santaguida, P.; Ismaila, A.; Patterson, C.; Cowan, D.; Levine, M.; Booker, L.; Oremus, M. *Ann. Int. Med.* **2008**, *148*, 379−397.

(8) Karran, E.; Mercken, M.; De Strooper, B. *Nat. Rev. Drug. Discuss.* **2011**, *10*, 698−712.

(9) Spies, P. E.; Slats, D.; Sjogren, J. M. C.; Kremer, B. P. H.; Verhey, F. R. J.; Rikkert, M.; Verbeek, M. M. *Curr. Alzheimer. Res.* **2010**, *7*, 470−476.

(10) Wogulis, M.; Wright, S.; Cunningham, D.; Chilcote, T.; Powell, K.; Rydel, R. E. *J. Neurosci.* **2005**, *25*, 1071−1080.

(11) Simard, A. R.; Soulet, D.; Gowing, G.; Julien, J. P.; Rivest, S. *Neuron* **2006**, *49*, 489−502.

(12) Brown, G. C.; Neher, J. J. *Mol. Neurobiol.* **2010**, *41*, 242−247.

(13) Meyer-Luehmann, M.; Spires-Jones, T. L.; Prada, C.; Garcia-Alloza, M.; de Calignon, A.; Rozkalne, A.; Koenigsknecht-Talboo, J.; Holtzman, D. M.; Bacskai, B. J.; Hyman, B. T. *Nature* **2008**, *451*, 720-U5.

(14) McLean, C. A.; Cherny, R. A.; Fraser, F. W.; Fuller, S. J.; Smith, M. J.; Beyreuther, K.; Bush, A. I.; Masters, C. L. *Ann. Neurol.* **1999**, *46*, 860−866.

(15) Lue, L. F.; Kuo, Y. M.; Roher, A. E.; Brachova, L.; Shen, Y.; Sue, L.; Beach, T.; Kurth, J. H.; Rydel, R. E.; Rogers, J. *Am. J. Pathol.* **1999**, *155*, 853−862.

(16) Gong, Y. S.; Chang, L.; Viola, K. L.; Lacor, P. N.; Lambert, M. P.; Finch, C. E.; Krafft, G. A.; Klein, W. L. *Proc. Natl. Acad. Sci. U.S.A.* **2003**, *100*, 10417−10422.

(17) Demuro, A.; Smith, M.; Parker, I. *J. Cell Biol.* **2011**, *195*, 515−524.

(18) Valincius, G.; Heinrich, F.; Budvytyte, R.; Vanderah, D. J.; McGillivray, D. J.; Sokolov, Y.; Hall, J. E.; Losche, M. *Biophys. J.* **2008**, *95*, 4845−4861.

(19) Arispe, N.; Diaz, J. C.; Simakova, O. *Biochim. Biophys. Acta, Biomembr.* **2007**, *1768*, 1952−1965.

(20) Arispe, N. *J. Membr. Biol.* **2004**, *197*, 33−48.

(21) Faendrich, M. *J. Mol. Biol.* **2012**, *421*, 427−440.

(22) Creed, M. C.; Milgram, N. W. *Age* **2010**, *32*, 365−384.

(23) Lee, J. S.; Ryu, J.; Park, C. B. *Anal. Chem.* **2009**, *81*, 2751−2759.

(24) Wei, C. W.; Peng, Y.; Zhang, L.; Huang, Q.; Cheng, M.; Liu, Y. N.; Li, J. *Bioorg. Med. Chem. Lett.* **2011**, *21*, 5818−5821.

(25) Huong Thi, V.; Shimanouchi, T.; Ishikawa, D.; Matsumoto, T.; Yagi, H.; Goto, Y.; Umakoshi, H.; Kuboi, R. *Biochem. Eng. J.* **2013**, *71*, 118−126.

(26) Ushikubo, H.; Watanabe, S.; Tanimoto, Y.; Abe, K.; Hiza, A.; Ogawa, T.; Asakawa, T.; Kan, T.; Akaishi, T. *Neurosci. Lett.* **2012**, *513*, 51−56.

(27) Ouberai, M.; Dumy, P.; Chierici, S.; Garcia, J. *Bioconjugate Chem.* **2009**, *20*, 2123−2132.

(28) Noor, H.; Cao, P.; Raleigh, D. P. *Protein Sci.* **2012**, *21*, 373−382.

(29) De Felice, F. G.; Vieira, M. N. N.; Saraiva, L. M.; Figueroa-Villar, J. D.; Garcia-Abreu, J.; Liu, R.; Chang, L.; Klein, W. L.; Ferreira, S. T. *FASEB J.* **2004**, *18*, 1366−1372.

(30) Veloso, A. J.; Dhar, D.; Chow, A. M.; Zhang, B.; Tang, D. W. F.; Ganesh, H. V. S.; Mikhaylichenko, S.; Brown, I. R.; Kerman, K. *ACS Chem. Neuro.* **2013**, *4*, 339−349.

(31) Veloso, A. J.; Chow, A. M.; Dhar, D.; Tang, D. W. F.; Ganesh, H. V. S.; Mikhaylichenko, S.; Brown, I. R.; Kerman, K. *ACS Chem. Neuro.* **2013**, *4*, 924−929.

(32) Wong, H. E.; Qi, W.; Choi, H. M.; Fernandez, E. J.; Kwon, I. *ACS Chem. Neuro.* **2011**, *2*, 645−657.

(33) Kayed, R.; Head, E.; Sarsoza, F.; Saing, T.; Cotman, C. W.; Necula, M.; Margol, L.; Wu, J.; Breydo, L.; Thompson, J. L.; Rasool, S.; Gurlo, T.; Butler, P.; Glabe, C. G. *Mol. Neurodegener.* **2007**, *2*, No. 10.1186/1750-1326-2-18.

(34) Hu, Y.; Su, B.; Kim, C. S.; Hernandez, M.; Rostagno, A.; Ghiso, J.; Kim, J. R. *ChemBioChem* **2010**, *11*, 2409−2418.

(35) Ladiwala, A. R. A.; Lin, J. C.; Bale, S. S.; Marcelino-Cruz, A. M.; Bhattacharya, M.; Dordick, J. S.; Tessier, P. M. *J. Biol. Chem.* **2010**, *285*, 24228−24237.

(36) Ehrnhoefer, D. E.; Bieschke, J.; Boeddrich, A.; Herbst, M.; Masino, L.; Lurz, R.; Engemann, S.; Pastore, A.; Wanker, E. E. *Nat. Struct. Mol. Biol.* **2008**, *15*, 558−566.

(37) Bonanni, A.; Pumera, M. *ACS Nano* **2011**, *5*, 2356−2361.

(38) Baur, J.; Gondran, C.; Holzinger, M.; Defrancq, E.; Perrot, H.; Cosnier, S. *Anal. Chem.* **2010**, *82*, 1066−1072.

(39) Barton, A. C.; Davis, F.; Higson, S. P. J. *Anal. Chem.* **2008**, *80*, 6198−6205.

(40) Castillo, G.; Trnkova, L.; Hrdy, R.; Hianik, T. *Electroanalysis* **2012**, *24*, 1079−1087.

(41) Cavalcanti, I. T.; Guedes, M. I. F.; Sotomayor, M. D. P. T.; Yamanaka, H.; Dutra, R. F. *Biochem. Eng. J.* **2012**, *67*, 225−230.

(42) Yu, H. Z. *Anal. Chem.* **2001**, *73*, 4743−4747.

(43) Escamilla-Gómez, V.; Campuzano, S.; Pedrero, M.; Pingarrón, J. M. *Biosens. Bioelectron.* **2009**, *24*, 3365−3371.

(44) Vallina-Garcia, R.; Garcia-Suarez, M. D.; Fernandez-Abedul, M. T.; Mendez, F. J.; Costa-Garcia, A. *Biosens. Bioelectron.* **2007**, *23*, 210−217.

(45) Viet, M. H.; Ngo, S. T.; Lam, N. S.; Li, M. S. *J. Phys. Chem. B* **2011**, *115*, 7433−7446.

(46) Veloso, A. J.; Kerman, K. *Bioelectrochemistry* **2012**, *84*, 49−52.

(47) Lopes, P.; Dyrnesli, H.; Lorenzen, N.; Otzen, D.; Ferapontova, E. E. *Analyst* **2014**, *139*, 749−756.

(48) Borsarelli, C. D.; Falomir-Lockhart, L. J.; Ostatna, V.; Fauerbach, J. A.; Hsiao, H. H.; Urlaub, H.; Palecek, E.; Jares-Erijman, E. A.; Jovin, T. M. *Free Radical Biol. Med.* **2012**, *53*, 1004−1015.

(49) Li, Y.; Ou, L. M. L.; Yu, H. Z. *Anal. Chem.* **2008**, *80*, 8216−8223.

(50) Wang, H.; Ou, L. M. L.; Suo, Y.; Yu, H. Z. *Anal. Chem.* **2011**, *83*, 1557−1563.

(51) Yu, H. Z.; Li, Y.; Ou, L. M. L. *Acc. Chem. Res.* **2013**, *46*, 258−268.

(52) Pallapa, M.; Ou, L. M. L.; Parameswaran, M.; Yu, H.-Z. *Sens. Actuat. B* **2010**, *148*, 620−623.

(53) Diomede, L.; Rigacci, S.; Romeo, M.; Stefani, M.; Salmona, M. *PLoS One* **2013**, *8*, No. 10.1371/journal.pone.0058893.

(54) Stravalaci, M.; Bastone, A.; Beeg, M.; Cagnotto, A.; Colombo, L.; Di Fede, G.; Tagliavini, F.; Cantu, L.; Del Favero, E.; Mazzanti, M.; Chiesa, R.; Salmona, M.; Diomede, L.; Gobbi, M. *J. Biol. Chem.* **2012**, *287*, 27796−27805.

(55) Zovo, K.; Helk, E.; Karafin, A.; Tõugu, V.; Palumaa, P. *Anal. Chem.* **2010**, *82*, 8558−8565.

(56) Sun, Y.; Zhang, G.; Hawkes, C. A.; Shaw, J. E.; McLaurin, J.; Nitz, M. *Biorg. Med. Chem.* **2008**, *16*, 7177−7184.

(57) Luhrs, T.; Ritter, C.; Adrian, M.; Riek-Loher, D.; Bohrmann, B.; Doeli, H.; Schubert, D.; Riek, R. *Proc. Natl. Acad. Sci. U.S.A.* **2005**, *102*, 17342−17347.

(58) Simmons, K. J.; Chopra, I.; Fishwick, C. W. G. *Nat. Rev. Microbiol.* **2010**, *8*, 501−510.

(59) Cosconati, S.; Forli, S.; Perryman, A. L.; Harris, R.; Goodsell, D. S.; Olson, A. J. *Expert Opin. Drug Discuss.* **2010**, *5*, 597−607.

(60) Ahmed, M.; Davis, J.; Aucoin, D.; Sato, T.; Ahuja, S.; Aimoto, S.; Elliott, J. I.; Van Nostrand, W. E.; Smith, S. O. *Nat. Struct. Mol. Biol.* **2010**, *17*, 561−567.